Nanomaterials and Energy
Volume 2 Issue NME4
Effect of a-Si:H–polymer interface on the behavior of hybrid solar cells
Mahadevapuram, Dalal and Chaudhary

ice | science

Pages 186–193 http://dx.doi.org/10.1680/nme.13.00014
Research Article
Received 07/06/2013 Accepted 16/07/2013
Published online 19/7/2013
Keywords: interfaces/polymers/solar cells

ice Institution of Civil Engineers
publishing

Effect of a-Si:H–polymer interface on the behavior of hybrid solar cells

1 **Rakesh C. Mahadevapuram** MS
Department of Materials Science and Engineering, Iowa State University, Ames, IA, USA

2 **Vikram L. Dalal** PhD
Department of Electrical and Computer Engineering, Iowa State University, Ames, IA, USA

3 **Sumit Chaudhary** PhD*
Department of Materials Science and Engineering, Iowa State University, Ames, IA, USA
Department of Electrical and Computer Engineering, Iowa State University, Ames, IA, USA

Organic photovoltaics (OPVs) are primary candidates for economical and flexible next-generation solar electricity conversion devices. However, efficiencies of the OPVs are limited, among other reasons, by poor charge transport and limited acceptor materials. To overcome this, hybrid organic–inorganic solar cells have been proposed. In this study, the authors investigated the photovoltaic characteristics of hybrid amorphous silicon (a-Si:H) films with varying doping nature with poly(3-hexylthiophene) (P3HT) only and P3HT:phenyl-C61-butyric acid methyl ester (PCBM) bulk-heterojunction–based solar cells. Both intrinsic and doped a-Si:H films were used. Despite the higher short circuit current density of P3HT/intrinsic a-Si:H device, the charge collection and open circuit voltage in P3HT/n+ a-Si:H device were the highest. This was attributed to favorable band bending and high built-in electric field in P3HT. Previously proposed model for photovoltaic mechanism in polymer/a-Si:H devices was revisited, and a revision was proposed. P3HT:PCBM cells on the three types of cells largely followed the same trend as the P3HT-only devices, except that intrinsic device did not have a photocurrent contribution from the organic layer.

1. Introduction

Over the last few decades, research on solution processable conjugated polymers has led to thrusts on extensive applications in electronic devices such as solar cells, light emitting diodes, photodetectors and transistors.[1] The band gap tunability along with high absorption coefficients of these conjugated polymers enables efficient photon capture in visible region of solar spectrum, leading to higher photocurrents. However, power conversion efficiency (PCE) in the organic photovoltaics (OPVs) suffers from, among other reasons, poor charge carrier mobilities in organic materials. Such mobilities are several orders lower than their inorganic counterparts. Moreover, although there are several electron-donor candidates in the typical donor:acceptor-type OPVs, acceptors are almost always fullerene derivatives. To alleviate these bottlenecks, hybridization of conjugated polymers with inorganic semiconductors, such as titanium dioxide, zinc oxide, cadmium selenide and silicon, has been conceptualized. Several such hybrid solar cells have been reported in the literature.[2–9]

Among the inorganic semiconductors, silicon is the least studied material system in organic–inorganic hybrid solar cells. However, in theory, it is promising because in itself silicon-only PV is a rather mature technology, absorption spectrum of silicon can be tuned by varying its amorphous or nanocrystalline nature, and its energy levels make it a potential competitor to fullerenes as an electron acceptor in hybrid solar cells.[9,10] Liu *et al.* reported on a Si:poly(3-hexylthiophene) (P3HT) bulk-heterojunction cells wherein silicon nanocrystals were blended with P3HT. Efficiencies between 1% and 1·5% were achieved; the devices mainly suffered from agglomeration of silicon nanocrystals.[9,11] Such an agglomeration in organic solvents is a common place when inorganic nanocrystals are not capped by organic ligands. Gowrishankar *et al.* investigated hybrid cells comprising conjugated polymers and hydrogenated amorphous silicon (a-Si:H) in the bilayer and ordered bulk configurations.[5,10] Efficiencies remained low; modeling and characterization revealed that photogenerated exciton in the polymer underwent energy transfer to a-Si:H, and the back hole transfer to polymer was not efficient due to holes being trapped in the valence band tail states of a-Si:H. Another hybrid silicon-organic embodiment that has been studied is where light absorption takes place only in the silicon layer, and a conducting polymer is used for transport of one of the charges (holes).[12] Motivated by the studies of Gowrinshankar *et al.*, the authors were further interested in the a-Si:H–polymer hybrid system because a-Si:H is the most mature

*Corresponding author e-mail address: sumitc@iastate.edu

thin-film silicon PV technology, and it absorbs strongly in the UV-blue region, which is complementary to most conjugated polymers. The complementary absorption aspect makes a-Si:H potentially suitable to be utilized in tandem cells with organics, with a-Si:H being the first subcell absorbing UV and blue, and polymeric system being the back cell absorbing green to near infrared. Two subcells in a tandem cell are connected via what is called a recombination layer or a tunnel junction. In a-Si:H and nanocrystalline silicon-based tandem cells, highly doped silicon (n+ and p+) layer is employed as a tunnel junction. Therefore, to explore beyond what was reported by Gowrishankar *et al*., the authors became interested in investigating how organics would interface with highly doped a-Si:H layers. That is the focus of this manuscript; till date there is no report on such interfaces. There is one report by Awasthi *et al*. in which they have described the role of n-type doping on the minority carrier (hole) recombination.[13] However, their focus was on designing higher performance hybrid Schottky solar cells by tuning the band-offsets across the n-type crystalline silicon-organic interface. Moreover, in their work, P3HT was used to utilize its conducting aspect only, rather than being a light-absorbing semiconductor.

In this study, the authors investigated the photovoltaic behavior of P3HT and P3HT:phenyl-C61-butyric acid methyl ester (PCBM) films on three types of a-Si:H films: (*1*) intrinsic, (*2*) highly p-type doped (p+) and (*3*) highly n-type doped (n+). In addition to current–voltage and quantum efficiency characterization, surface roughnesses were also characterized. Band diagrams were utilized to understand the observed photovoltaic behavior.

2. Experimental

For the transparent substrate, 50 nm of high-conductivity 2 wt% aluminium-doped zinc oxide thin films was deposited on the glass substrates in the radio frequency (RF)-sputtering unit at 100-W power, 150°C substrate temperature and 5-mT chamber pressure conditions. These substrates were found to be transparent in the visible wavelength range from UV-Vis absorbance measurements and annealing at 200°C for 20 min was prformed to improve their sheet conductivity. Subsequently, these substrates were transferred to plasma-enhanced chemical vapor deposition chamber operated at radio frequency (RF) of 45 MHz. a-Si:H films were deposited by using precursor gases of silane and hydrogen in a flow ratio of 1:10. Dopant gases include diborane and trimethylborane for p+ layer and phosphine for n+ layer. The RF forward power was maintained at 6–6·5 W, and the substrate temperatures at 300 and 225°C for instrinsic/n+ and p+ layers, respectively. The chamber pressures were maintained at 100 and 50 mT for instrinsic and n+/p+ a-Si:H layers, respectively. The deposition times were optimized to control the thicknesses for each of these layers to obtain 100/30/50 nm of intrinsic/n+/p+ a-Si:H, respectively. For set 1 consisting of P3HT/a-Si-based devices, the substrates were spin coated with 20 mg/ml of P3HT in 1,2-dichlorobenzene at 1000 rpm and solvent annealed for 1 h. For the set 2 devices of P3HT:PCBM/a-Si:H, the substrates were spin coated with 20-mg/ml (1:1 weight ratio) mixture of P3HT:PCBM in 1,2-dichlorobenzene at 600 rpm, and solvent annealed in a petri dish for 1 h inside an nitrogen-filled glove box. The dried films were then transferred to thermal evaporator, and 200 nm of silver was deposited as the top electrode. Thereafter, the devices were thermally annealed at 120°C to improve the crystallinity of the polymer films and improve the organic-electrode interfacial contact.[14–20] To measure the photocurrent versus voltage, devices were illuminated using ELH quartz line lamp operating at 1 SUN intensity, that is, 100 mW/cm^2 calibrated using crystalline silicon photodiode with a KG-5 filter. External quantum efficiency (EQE) measurements were also performed using this lamp and a monochromator with a lock-in amplifier to eliminate background noise. The reference was a calibrated silicon photodiode with known EQE spectra. The absorption spectra of the films were measured in Varian Cary 5000 UV-Vis-NIR spectrophotometer (Agilent Technologies, CA, USA). Veeco's Digital Instruments AFM (Bruker, CA, USA) in tapping mode was used to characterize surface morphology.

3. Results and discussion

Device architecture of planar heterojunction bilayer solar cells of P3HT (or P3HT:PCBM)/a-Si:H hybrid solar cells is depicted in Figure 1(a). Here, the bilayer active layer of P3HT (or P3HT:PCBM) and a-Si:H is sandwiched between aluminium-doped zinc oxide at the bottom transparent conducting bottom electrode and several small area silver electrodes as top contacts. Energy band diagram of P3HT/a-Si:H (intrinsic) is schematically represented Figure 1(b) to depict the presence of tail states in this type-II heterojunction. Variation in Fermi-level splitting upon illumination leads to differences in V_{oc} observed across P3HT/a-Si:H interface due to the presence of tail states in a-Si:H. However, when excess amounts of dopants (boron or phosphorous) are introduced in a-Si:H layer, the electronic behavior shifts to that of metal whose work function (WF) is defined by the Fermi level either near valence band edge or the conduction band edge. Current–voltage characteristics under illumination are plotted in Figure 1(c), and in both intrinsic- and n+-based devices, the saturation of photocurrent at low reverse bias could be observed. For p+-based device, the J-V trend is linear in nature similar to a resistor with photocurrent increasing with bias in the reverse direction. Table 1 shows photovoltaic parameters of these devices.

From Table 1, it is observe the PCE of the P3HT/instrinsic a-Si:H solar cell is the best despite lower V_{oc} than n+ device. This is because of higher J_{sc} in intrinsic device, whereas n+/p+ layers have negligible contribution to photocurrent generation. From Figure 1(c), it is observed that FFs are comparatively better in instrinsic and n+ sample than p+ sample, owing to better shunt resistance as observed by the slope of J-V curve at short circuit conditions. Further explanation is provided below from the point of view of band diagrams.

Figure 1(d) shows the EQE plots of all three devices. EQE plots show that only intrinsic a-Si:H device has photocurrent contribution from silicon, as apparent from the rising tail in the 400–450-nm region that matches with the a-Si:H absorption.[5] The contribution between 450 and 650 nm comes from P3HT layer and corresponds to the P3HT absorption. p+ and n+ devices do not contribute to photocurrent from a-Si:H layer, which is not surprising because the high dopant concentration leads to near complete recombination of minority carriers. As a result, the short circuit current density is highest in intrinsic devices.

Differences in open circuit voltages (V_{oc})s for the above three devices can be illustrated with the help of following band diagrams at short circuit condition as shown in Figure 2(a)–2(c).

The highly doped n+ and p+ a-Si:H layers can be considered to be metals due to their high carrier concentrations, and their WFs are defined by the position of the Fermi levels as shown in Figure 2(b) and 2(c). The built-in electric field in case of P3HT/n+ a-Si:H device (WF difference between silver and silicon is 1 eV) is the highest and in case of P3HT/p+ a-Si:H is the lowest (WF difference

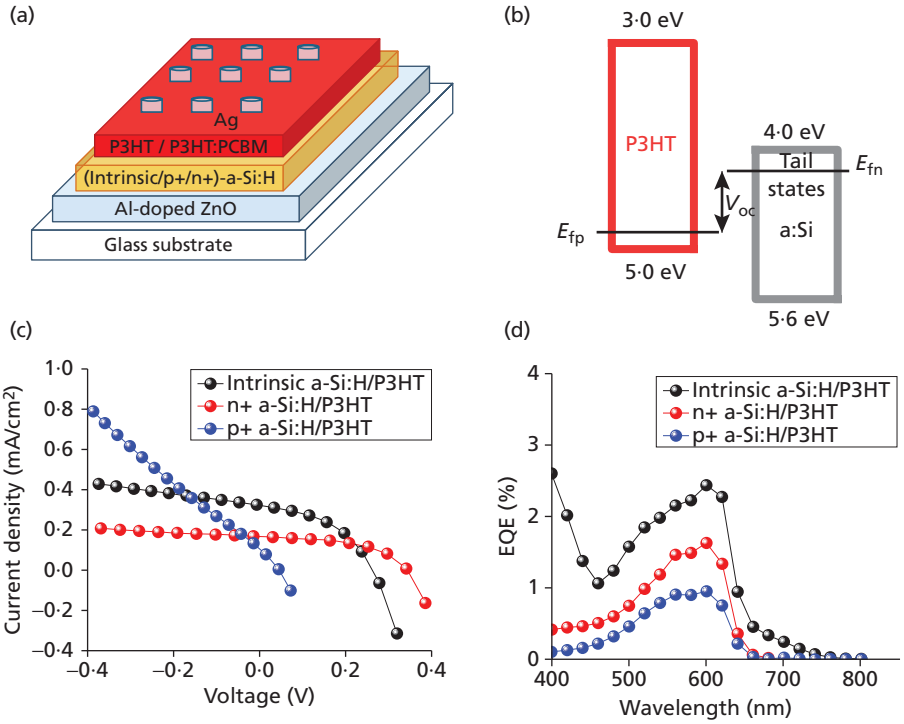

Figure 1. (a) Schematic of bilayer device architecture for hybrid P3HT/(P3HT:PCBM)/a-Si:H solar cells for different doping levels. (b) Schematic of energy band diagram of bilayer heterojunction solar cells of P3HT/a-Si:H with tail states. (c) J-V characteristics of P3HT/a-Si:H hybrid solar cells under AM 1·5G conditions with 1 SUN incident intensity. (d) EQE of the P3HT/a-Si:H hybrid solar cells. a-Si:H, hydrogenated amorphous silicon; P3HT, poly(3-hexylthiophene); PCBM, phenyl-C61-butyric acid methyl ester.

Photovoltaic parameter	P3HT/intrinsic a-Si:H	P3HT/n+ a-Si:H	P3HT/p+ a-Si:H
J_{sc} (mA/cm²)	0·30	0·15	0·09
V_{oc} (V)	0·27	0·35	0·04
FF (%)	45·38	51·86	27·13
PCE (%)	0·036	0·027	0·001

FF, fill factor; J_{sc}, Short circuit current; PCE, power conversion efficiency; V_{oc}, Open circuit voltage.

Table 1. Photovoltaic parameters of P3HT/a-Si:H (intrinsic, n+ and p+) hybrid solar cells.

between silver and silicon is 0·5 eV), which is reflected in the V_{oc} values. Moreover, in p+ a-Si:H device, the direction of band bending favors electron transport to silver electrode and hole transport to the p+ a-Si:H contact. However, the holes generated/transported from the bulk to the silicon-P3HT interface will be trapped due to the formation of a Schottky junction as shown in Figure 2(c), resulting in severe recombination losses and lowest value of V_{oc}. In the P3HT/intrinsic a-Si:H sample as shown in Figure 2(a), V_{oc} is limited by the interface gap between a-Si:H and P3HT due to quasi-Fermi levels pinning by the tail states. Thus, intrinsic a-Si:H

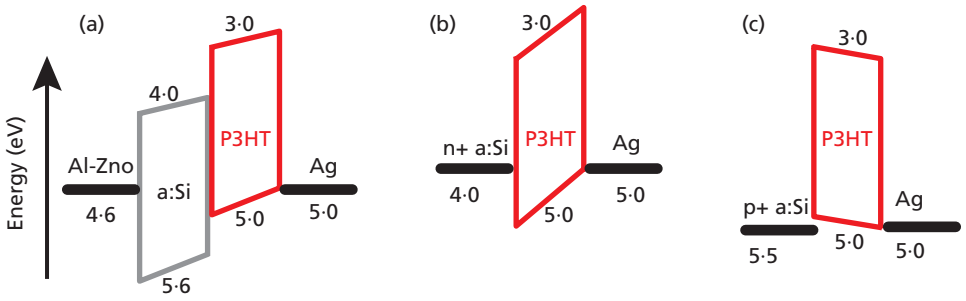

Figure 2. Energy band diagrams of the bilayer (a) P3HT/intrinsic a-Si:H (b) P3HT/n+ a-Si:H and (c)P3HT/p+ a-Si:H hybrid solar cells at short circuit condition. a-Si:H, hydrogenated amorphous silicon; P3HT, poly(3-hexylthiophene).

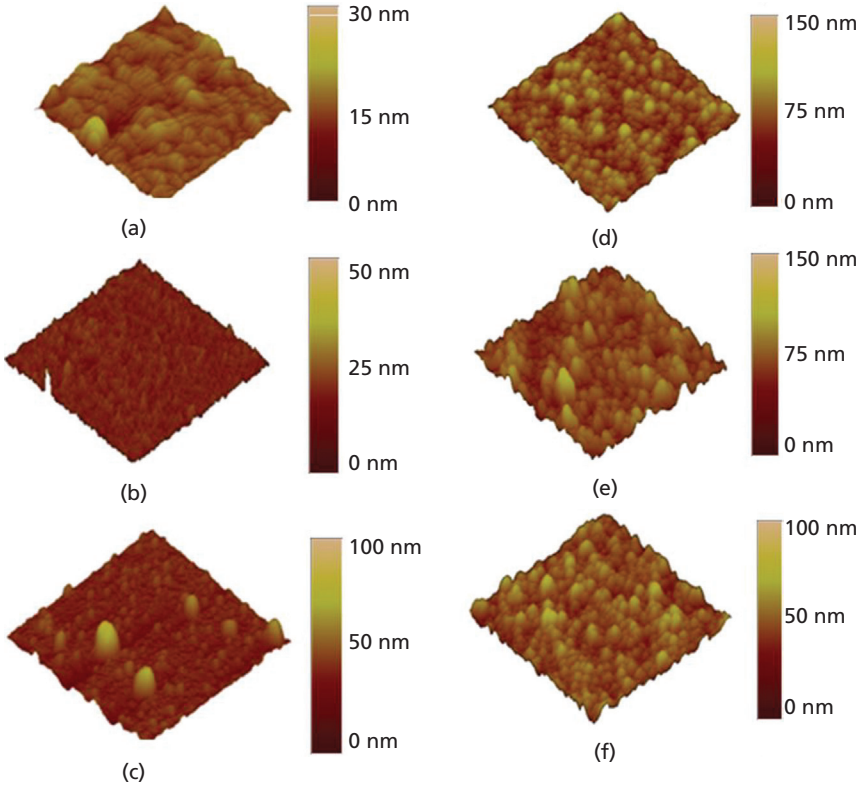

Figure 3. AFM 3D height images (a) bare intrinsic a-Si:H (b) bare n+ a-Si:H (c) bare p+ a-Si:H (d) P3HT film on intrinsic a-Si:H (e) P3HT film on n+ a-Si:H (f) P3HT film on p+ a-Si:H. The scan size was fixed at 5 μm × 5 μm in all the cases and tapping mode was used to obtain the surface morphology images. a-Si:H, hydrogenated amorphous silicon; P3HT, poly(3-hexylthiophene).

devices has less V_{oc} than the n+ devices. Since fill factor (FF) is indirectly linked to V_{oc}, FF values also follow the same trend as the V_{oc} values. FF of n+ device is ~10% better than the intrinsic device because in addition to higher built-in field as shown in the band diagrams, n+ device does not suffer from the problem of holes being trapped in the tail states of a-Si:H. They simply get transported from the P3HT phase to silver anode.

Surface morphology of the different layers in such bilayer thin-film solar cells is important, and AFM characterization was used to obtain 3D images of surfaces for these films as shown in Figure 3. Quantitative assessment of the surface morphology can be done by measuring root-mean-squared (RMS) roughness (σ_{rms}) from the AFM height images. From Table 2, it can be seen that σ_{rms} of bare p+ a-Si:H and the overlying P3HT film is the highest in all three samples. This is another reason that can contribute to the worst performance of p+ devices. p+ film shows several high spots that can act as shunt paths and lead to high recombination leakage currents. Qualitatively the surface morphology of the P3HT films does not vary much with the nature of the underlying substrate, and this is indicated by the similar values of σ_{rms} for P3HT layer.

The results of this study also shed light on the photovoltaic mechanism in these devices. Gowrishankar *et al*. proposed that after the light is absorbed in the polymer and exciton is created, it is not the electron that transfers to a-Si:H but rather the entire exciton via Forster resonance energy transfer, and then, the hole is transferred back to the polymer.[5] However, if this was entirely the case, the authors will not expect the J_{sc} of their n+ device to be as high as 50% of intrinsic device. This is because upon energy transfer, the holes will be minority carriers in the n+ a-Si:H layer and will have negligible chance of making it back to P3HT. A good portion of 50% loss is attributed to lack of photocurrent contribution from a-Si:H, and it seems that the holes originally belonging to P3HT are safely transported outside. Thus, though the authors entirely do not disagree with Gowrishankar *et al*., their results strongly indicate that in addition to FRET-type energy transfer, if any, direct electron transfer from P3HT to a-Si:H also takes place, and the hole stays within the P3HT phase and get transported to silver anode.

From the above discussion, it can be seen that hybrid solar cells of P3HT with a-Si:H-based films showed very low J_{sc}, and this was the primary reason behind low PCEs. This is evidently due to the bottleneck of the bilayer heterojunction structure, that the exciton harvesting in the polymer is incomplete due to small exciton dissociation lengths (~10 nm). Thus, excitons >10 nm or so away from the silicon-organic or organic-metal interface are not harvested. To improve exciton harvesting, the authors fabricated P3HT:PCBM cells on the three types of silicon films. The authors

Nature of a-Si:H	Surface roughness (σ_{ms}) of bare a-Si:H (nm)	Surface roughness (σ_{ms}) of P3HT film on a-Si:H	Short circuit current density (J) in mA/cm²
Intrinsic a-Si:H	2·57	6·85	0·3
n+ a-Si:H	3·5	8·24	0·15
p+ a-Si:H	10·31	8·6	0·09

Table 2. Comparision of σ_{rms} obtained from AFM 3D height images of a-Si:H and P3HT/a-Si:H films and their correlation to short circuit density.

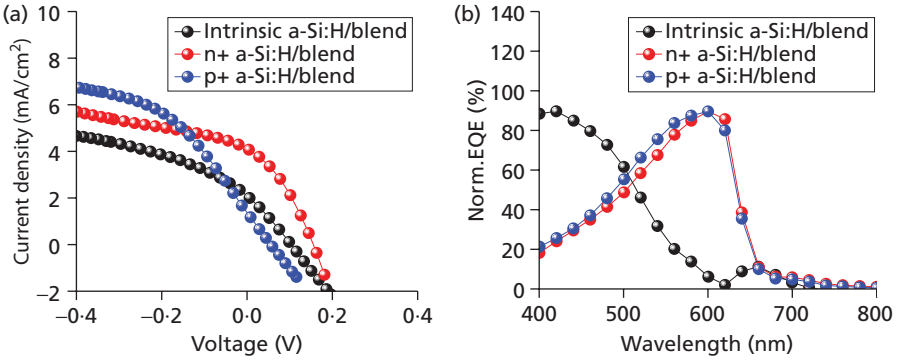

Figure 4. (a) J-V characteristics of a-Si:H/blend (P3HT:PCBM mixture) hybrid solar cells under AM 1·5G conditions with 1 SUN incident intensity (b) EQE of the a-Si:H/blend hybrid solar cells. a-Si:H, hydrogenated amorphous silicon; P3HT, poly(3-hexylthiophene); PCBM, phenyl-C61-butyric acid methyl ester.

hypothesized that in such devices, excitons throughout the organic layer will split at the P3HT:PCBM interfaces. The authors were then interested in observing the charges that reach the organic-silicon interface.

A bulk-heterojunction blend of P3HT:PCBM was spin coated over different a-Si:H substrates (n+/p+/intrinsic a-Si:H), and the devices were tested under 1 SUN intensity conditions. The J-V curves under 1 SUN irradiation, and normalized quantum efficiency curves are shown in Figure 4 and the corresponding energy band diagrams of these devices are depicted in Figure 5. Photovoltaic parameters are listed in Table 3.

As expected, current densities for all the devices increased as compared with the P3HT-a-Si:H devices discussed above. As shown by the photocurrent–voltage curves in Figure 4(a), n+ a-Si:H-based device showed best V_{oc}, J_{sc} and FF and hence highest PCE. The higher PCE in case of P3HT:PCBM/n+ a-Si:H can be explained by the extent of favorable band bending shown in Figure 5(b). However, P3HT:PCBM/p+ a-Si:H devices suffer from significant recombination losses similar to P3HT/p+ a-Si:H bilayer hybrid devices, and this phenomena can be attributed to unfavorable band-bending characteristics as shown in Figure 5(c).

Any increase in photocurrent with high reverse bias is indicative of high barrier to charge collection (low FF), and this is observed in J-V curve for P3HT:PCBM/p+ a-Si:H device (blue spheres) as shown in Figure 4(a). One would expect the bilayer device of P3HT:PCBM with instrinsic a-Si:H to result in higher photocurrent due to complementary absorption characteristics of instrinsic a-Si:H and blend. However, it can be observed from normalized QE plot given in Figure 4(b) that there is negligible QE response in 500–650 nm wavelength range corresponding to P3HT:PCBM blend.

From Figure 5(c), it can be seen that the direction of band bending is unfavorable for charge transport in P3HT (hole) and PCBM (electron) layers leading to recombination losses at interface. It is currently unclear as to why P3HT:PCBM/instrinsic a-Si:H device shows lower J_{sc}, when compared with that of P3HT:PCBM/n+ a-Si:H device. One of the possible reasons could be high barrier to charge collection reflected in high series resistance – bulk resistance from active layers leading to recombination losses and contact resistances. Moreover, on the basis of the energy band diagram in Figure 5(a), it can be concluded that the difference in WFs of the electrodes is insufficient and does not lead to high built-in electric field leading to lower V_{oc} in the P3HT:PCBM/instrinsic a-Si:H device. These results show that P3HT:PCBM/n+ a-Si:H has the

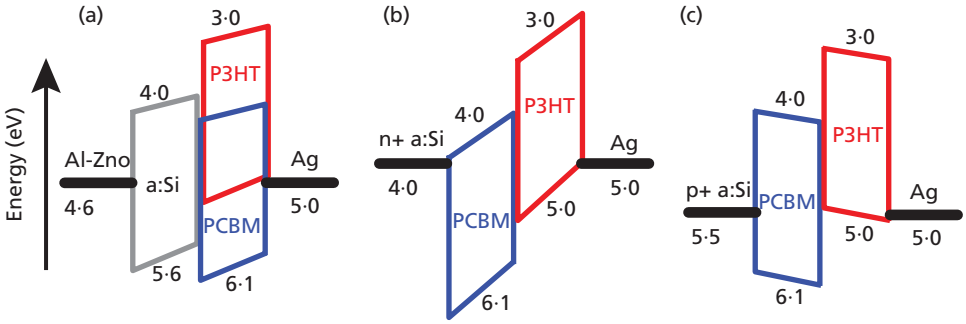

Figure 5. Energy band diagrams of the bilayer (a) P3HT:PCBM/intrinsic a-Si:H (b) P3HT:PCBM/n+ a-Si:H and (c) P3HT:PCBM/p+ a-Si:H hybrid solar cells at short circuit condition. a-Si:H, hydrogenated amorphous silicon; P3HT, poly(3-hexylthiophene); PCBM, phenyl-C61-butyric acid methyl ester.

Photovoltaic parameter	P3HT:PCBM/intrinsic a-Si:H	P3HT:PCBM/n+ a-Si:H	P3HT:PCBM/p+ a-Si:H
J_{sc} (mA/cm^2)	1·91	3·94	0·37
V_{oc} (V)	0·11	0·15	0·02
FF (%)	27·8	34·3	24·4
PCE (%)	0·05	0·21	0·011

FF, fill factor; J_{sc}, Short circuit current; PCE, power conversion efficiency; V_{oc}, Open circuit voltage.

Table 3. Photovoltaic parameters of P3HT:PCBM/a-Si:H hybrid solar cells obtained from Figure 4(a) corresponding to (n+/p+/instrinsic) a-Si:H films.

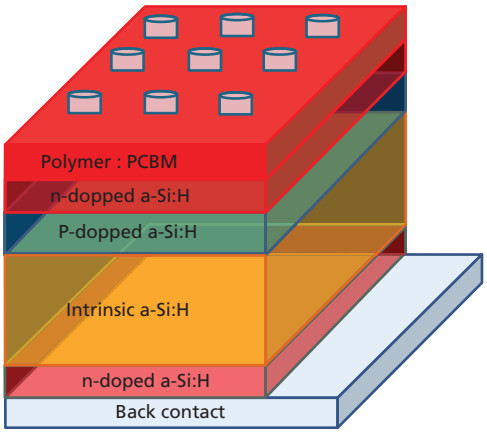

Figure 6. Schematic of tandem architecture with n+ a-Si:H as the favorable electrode for the top polymer:fullerene subcell. a-Si:H, hydrogenated amorphous silicon.

potential to be a subcell in a silicon-organic tandem photovoltaic cell, with n+ layer being one of the two legs of the tunnel junction. A diagram of the conceptualized tandem cell is shown in Figure 6.

4. Conclusions

In P3HT/a-Si:H hybrid solar cells, the authors found that n-type doping in a-Si:H part of the device is suitable for high V_{oc} but does not contribute significantly to photocurrent generation. n-type doping in a-Si:H layer also leads to higher FF indicated by the favorable band bending and charge collection shown in the band diagrams. Topography of a-Si:H is also a critical parameter in the determination of electronic behavior, as p+ a-Si:H film has surface roughness that could lead to high shunts responsible for high leakage currents. These results show that in silicon-polymer system, there is not only energy transfer from the polymer to silicon but also direct electron transfer from polymer to silicon. For the design of double-junction solar cells, the authors believe that the combination of highly doped p-n junction as the tunnel junction would be a novel concept for silicon-polymer tandem cells.

Acknowledgements

This material is based upon work supported by the National Science Foundation under Grant Number (ECCS-1055930).

REFERENCES

1. Sirringhaus, H. Organic semiconductors: an equal-opportunity conductor. *Nature Materials* **2003**, *2*(10), 641–642.
2. Breeze, A.; Schlesinger, Z.; Carter, S.; Brock, P. Charge transport in TiO_2/MEH-PPV polymer photovoltaics. *Physical Review B* **2001**, *64*(12), 125205.
3. Coakley, K. M.; McGehee, M. D. Photovoltaic cells made from conjugated polymers infiltrated into mesoporous titania. *Applied Physics Letters* **2003**, *83*(16), 3380–3382.
4. Garnier, F. Hybrid organic-on-inorganic photovoltaic devices. *Journal of Optics A: Pure and Applied Optics* **2002**, *4*(6), S247.
5. Gowrishankar, V.; Scully, S. R.; Chan, A. T.; McGehee, M. D.; Wang, Q.; Branz, H. M. Exciton harvesting, charge transfer, and charge-carrier transport in amorphous-silicon nanopillar/polymer hybrid solar cells. *Journal of Applied Physics* **2008**, *103*(6), 064511–064518.
6. Huynh, W. U.; Dittmer, J. J.; Alivisatos, A. P. Hybrid nanorod-polymer solar cells. *Science* **2002**, *295*(5564), 2425–2427.
7. Kwong, C.; Djurišić, A.; Chui, P.; Cheng, K.; Chan, W. Influence of solvent on film morphology and device performance of poly (3-hexylthiophene): TiO_2 nanocomposite solar cells. *Chemical Physics Letters* **2004**, *384*(4), 372–375.
8. Levitsky, I.; Euler, W.; Tokranova, N.; Xu, B.; Castracane, J. Hybrid solar cells based on porous Si and copper phthalocyanine derivatives. *Applied Physics Letters* **2004**, *85*(25), 6245–6247.
9. Liu, C.-Y.; Holman, Z. C.; Kortshagen, U. R. Hybrid solar cells from P3HT and silicon nanocrystals. *Nano Letters* **2008**, *9*(1), 449–452.
10. Gowrishankar, V.; Scully, S. R.; McGehee, M. D.; Wang, Q.; Branz, H. M. Exciton splitting and carrier transport across the amorphous-silicon/polymer solar cell interface. *Applied Physics Letters* **2006**, *89*(25), 252102–252103.
11. Liu, C. Y.; Holman, Z. C.; Kortshagen, U. R. Optimization of Si NC/P3HT hybrid solar cells. *Advanced Functional Materials* **2010**, *20*(13), 2157–2164.
12. Shen, X.; Sun, B.; Liu, D.; Lee, S.-T. Hybrid heterojunction solar cell based on organic–inorganic silicon nanowire array architecture. *Journal of the American Chemical Society* **2011**, *133*(48), 19408–19415.
13. Avasthi, S.; Lee, S.; Loo, Y. L.; Sturm, J. C. Role of majority and minority carrier barriers silicon/organic hybrid heterojunction solar cells. *Advanced Materials* **2011**, *23*(48), 5762–5766.
14. Zen, A.; Pflaum, J.; Hirschmann, S.; Zhuang, W.; Jaiser, F.; Asawapirom, U.; Rabe, J. P.; Scherf, U.; Neher, D. Effect of molecular weight and annealing of poly (3-hexylthiophene) s on the performance of organic field-effect transistors. *Advanced Functional Materials* **2004**, *14*(8), 757–764.
15. Joshi, S.; Pingel, P.; Grigorian, S.; Panzner, T.; Pietsch, U.; Neher, D.; Forster, M.; Scherf, U. Bimodal temperature behavior of structure and mobility in high molecular weight P3HT thin films. *Macromolecules* **2009**, *42*(13), 4651–4660.
16. Hiorns, R. C.; De Bettignies, R.; Leroy, J.; Bailly, S.; Firon, M.; Sentein, C.; Khoukh, A.; Preud'homme, H.; Dagron-Lartigau, C. High molecular weights, polydispersities, and annealing temperatures in the optimization of bulk-heterojunction photovoltaic cells based on poly (3-hexylthiophene) or poly (3-butylthiophene). *Advanced Functional Materials* **2006**, *16*(17), 2263–2273.

17. Dang, M. T.; Hirsch, L.; Wantz, G.; Wuest, J. D. Controlling the morphology and performance of bulk heterojunctions in solar cells. lessons learned from the benchmark poly (3-hexylthiophene):[6, 6]-phenyl-c61-butyric acid methyl ester system. *Chemical Reviews* **2013**.
18. Li, G.; Shrotriya, V.; Yao, Y.; Yang, Y. Investigation of annealing effects and film thickness dependence of polymer solar cells based on poly (3-hexylthiophene). *Journal of Applied Physics* **2005**, *98*(4), 043704–043705.
19. Liu, J.; Shi, Y.; Yang, Y. Solvation-induced morphology effects on the performance of polymer-based photovoltaic devices. *Advanced Functional Materials* **2001**, *11*(6), 420.
20. Hoppe, H.; Niggemann, M.; Winder, C.; Kraut, J.; Hiesgen, R.; Hinsch, A.; Meissner, D.; Sariciftci, N. S. Nanoscale morphology of conjugated polymer/fullerene-based bulk-heterojunction solar cells. *Advanced Functional Materials* **2004**, *14*(10), 1005–1011.